FLUTTER ANALYSIS OF PIEZOELECTRIC BEAMS IN MEMS

Raffaele Ardito[+1] and Rocco Musci[+1]
[+1] Department of Civil and Environmental Engineering, Politecnico di Milano, Milan, Italy

Micro-electro-mechanical systems (MEMS) represent a huge class of devices characterized by the smart coupling between electronics and mechanics, in order to obtain microscopic sensors and actuators. The use of piezoelectric materials in MEMS is steadily increasing, considering both the "direct effect", e.g. in energy harvesters, and the "indirect effect", for the cases of resonators, micropumps and other actuators. This paper is devoted to the study of piezoelectric laminate beams in the presence of aeroelastic effects due to the interaction of the structure with a fluid flow, as it may happen if the MEMS is embedded in a fluidic system. More specifically, the analytical conditions for the onset of flutter instability are studied, with the purpose of providing a sound basis for further studies focused on energy harvesting from fluid flows.

Keyword: micro-electro-mechanical systems, fluid-structure interaction, aeroelasticity, piezoelectric behavior, energy harvesting.

1. INTRODUCTION

The world of micro-electro-mechanical systems (MEMS) is currently expanding by means of the inclusion of piezoelectric materials, which can be embedded in the manufacturing process in the form of thin films[1)]. The conversion of mechanical energy into electrical one can be used in order to harvest (or scavenge) small amounts of energy from ambient vibrations[2)]. A scavenged power of the order of microWatts can be sufficient to feed MEMS sensors, with the aim of eliminating batteries or complex wiring in microsystems, thus moving a step closer towards battery-less, autonomous sensors systems and networks which recover on-site the energy they need to fulfill their tasks.

For MEMS energy harvesters, piezoelectric transduction is the most appropriate scenario since standard MEMS thin-film processes are available for many piezoelectric materials assuring high efficiency, high energy density and scalability. Operating frequency, frequency bandwidth, excitation level, power density and size are the key design function requirements. Cantilever laminated beams with thin films of lead zirconate titanate $Pb(Zr,Ti)O_3$ (PZT) have been widely used as linear resonating harvesters achieving high power generation. The multi-physics simulation of piezoelectric effect can be obtained by considering that the structural members are represented by a laminate composite with piezoelectric and silicon layers; the piezoelectric material is then attached to an external circuitry, which reproduces the device employed for the power management.

The energy source for MEMS harvester is commonly represented by ambient vibration: in that case, the micro-device is basically an inertial transducer, endowed with a large mass in order to emphasize the kinetic energy[3)]. Such systems are characterized by a severe discrepancy between the natural frequency and the excitation frequency, so that some specific provisions should be introduced in order to force a resonating behaviour (frequency-up-conversion). In this paper, a different scenario is considered: the possibility of energy harvesting from fluid flow is explored, with the exploitation of aeroelastic phenomena (such as the vortex induced vibration, thoroughly studied in our previous work[4)]). This paper is specifically focused on the theoretical and computational analysis of Flutter Instability (FI[5)]) for piezoelectric beams in MEMS, with the main purpose of establishing the solution procedure and achieving some preliminary results. In view of its ability to reduce the dissipative component, flutter behavior can be exploited for the energy harvesting purpose, joining this aeroelastic phenomenon with another type of excitation, like an inertial forcing.

In our multi-physics simulations, the structural members are represented by laminate composites with

[+1]raffaele.ardito@polimi.it, muscirocco@gmail.com

piezoelectric and silicon layers, the active layer being attached to an external circuitry. The sectional behavior of the beam is studied through the Classical Lamination Theory (CLT, specifically modified in order to introduce the piezoelectric coupling[6]) and a reduced order model is built through separation of time and space variables. The theoretical study has been based on reduced order models, obtained by applying the Rayleigh-Ritz method. The preliminary simulations, carried out in the present study, allow for a deeper understanding of energy harvesting from fluid flow at the micro-scale. The achieved results will be used, in future works, in order to obtain optimized devices, possibly endowed with different and more complex shapes with respect to the simple cantilever considered herein.

The paper is organized as follows. Section 2 contains a detailed explanation of the mechanical model for a piezoelectric composite beam subject to aeroelastic effects. Section 3 is devoted to the description of the simple device, which is studied as a paradigm of a class of realistic MEMS. Section 4 contains the main results in terms of the assessment of FI and Section 5 is referred to the possible application in the field of energy harvester. Some conclusive remarks and future prospects are drawn in Section 6.

2. MULTI-PHYSICS MODEL OF LAYERED PIEZOELECTRIC BEAMS

(1) Mechanical and electrical model

The paper deals with layered piezoelectric beams, such as the simple cantilever shown in Fig. 1. It is worth noting that realistic piezoelectric beams include many different layers, among which the upper and the lower electrodes for the active layer. In view of the limited thickness of ancillary layers, in this preliminary study a simplified geometry is considered, with a structural layer (e.g. made of silicon) and a piezoelectric layer (e.g. made of PZT). In what follows, l is the length, t is the total thickness and t_p is the thickness of PZT layer, b is the width. The origin of the reference system is located on the clamped-in edge, in correspondence of the neutral axis of the cross-section.

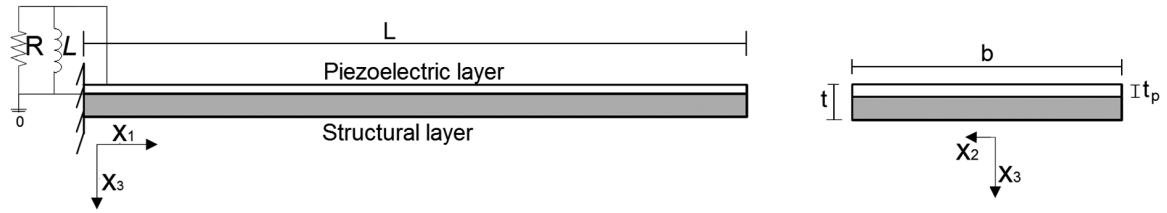

Figure 1: Schematic views of the considered beam: lateral view, along with the external RL circuit, and cross-section view.

The piezoelectric layer is polarized in the vertical direction (i.e. along the x_3 axis) and it works in the so-called “d31-mode” when the beam vibrates: this means that the deformation along x_1 axis causes an electric field along the x_3 axis. In order to implement the d31-mode, the electrodes span both upper and lower surfaces of PZT thin film.

Considering that the structural member is represented by a laminate composite, the sectional behavior of the beam is studied through the Classical Lamination Theory specifically modified in order to introduce the piezoelectric coupling[7]. The beam is sufficiently thin and slender, so that Bernoulli’s assumptions can be adopted: the rotation of the cross section is the derivative of the vertical displacement (w_3) and the horizontal displacement (s_1) and strain (S_{11}) read (in the standard notation for piezoelectricity[8]) :

$$s_1(x_1,x_3) = -x_3 \frac{\partial w_3(x_1)}{\partial x_1} \qquad S_{11}(x_1,x_3) = -x_3 \frac{\partial^2 w_3(x_1)}{\partial x_1^2} \tag{1}$$

The electric potential is constant over the electrodes: the potential value is assigned on the bottom electrode (grounded electrode) and it is free to change on the upper one (v). According to the piezoelectric constitutive law, the electric field is proportional to strain, which is linear across the piezoelectric layer thickness. Consequently, the electric potential across the thickness of the piezoelectric layer, denoted by $\phi(x_3)$,

should be a quadratic function of x_3. However, as long as the piezoelectric layer is thin, a linear approximation of the potential can be adopted, so that the electric field E_3 turns out to be constant:

$$\phi(x_3) = -\frac{x_3{}^*}{t_p} v \qquad E_3(x_1, x_3) = -\frac{\partial \phi(x_3)}{\partial x_3} = \frac{v}{t_p} \tag{2}$$

where the axis $x_3{}^*$ axis has the same direction as x_3 but its origin is located on the interface between the two layers. A piezoelectric constitutive law is employed herein to describe strain-stress relation; the fully-coupled law for d31-mode reads:

$$T_{11} = c_1 S_{11} - e_{31} E_3 \qquad D_3 = e_{31} S_{11} + \varepsilon_3^s E_3 \tag{3}$$

In Eq. 3, T_{11} and S_{11} are the stress and strain components along the axis x_1; D_3 and E_3 are the electric displacement and the electric field components along the axis x_3 and c_1, e_{31} and $\varepsilon_3{}^s$ are the elastic, piezoelectric and dielectric constant, respectively.

By considering the integration across the thickness, one obtains the generalized parameters in terms of stiffness, piezoelectric coupling coefficient and electrical capacitance[9]. In order to describe the beam deflection, the Rayeigh-Ritz method is adopted. The deformed shape is governed by a single parameter, namely the tip displacement $w(t)$:

$$w_3(x_1, t) = w(t) \psi_w(x_1) \tag{4}$$

The accuracy of this approximate method will be discussed in the next Section.

Through the principle of virtual power and using the assumptions herein adopted, the dynamic equilibrium equations of the coupled system results:

$$\begin{cases} m\ddot{w} + c\dot{w} + kw - \Theta v = f \\ C_E v + \Theta w = q \end{cases} \tag{5}$$

The above equation describes the dynamic behavior of the linear piezoelectric beam. The coefficients are evaluated by integrating the shape functions and the generalized constitutive coefficients on the area of the beam: m is the total mass, k is the linear elastic stiffness, C_E is the internal capacitance of PZT and Θ is the linear coupling coefficient.

The electric charge collected by the electrodes is managed by an external electric circuit. Two kinds of circuits are analyzed: a purely resistive solution (RC) and a resistive-inductive one (RLC)[10]. The resistor and the inductor are governed by the laws:

$$i_R = \dot{q} = -\frac{v}{R} \qquad \frac{d(i_L)}{dt} = \ddot{q} = -\frac{v}{L} \tag{6}$$

Therefore, the second expression in Eq. (5) becomes, for RC case:

$$C_E \dot{v} + \Theta \dot{w} + \frac{v}{R} = 0 \tag{7}$$

and for RLC case:

$$C_E \ddot{v} + \Theta \ddot{w} + \frac{\dot{v}}{R} + \frac{v}{L} = 0 \tag{8}$$

where R and L are the value of load resistance and inductance, respectively.

(2) Aeroelastic model

In this paper, the so-called classical flutter instability is analyzed. In a simple mechanical model, this aeroelastic phenomenon is characterized by two degrees of freedom, rotation and vertical translation, coupled in a flow-driven, unstable oscillation. According to the features of the instability mechanisms, the motion of the structure will either decay or diverge according to whether the energy of motion extracted from the flow is less than or exceeds the energy dissipated by the system through mechanical damping. The border that divides these two conditions is eventually recognized as the critical flutter condition.

When a piezoelectric beam is considered, the equations of motion should include also the effect of the

electric potential in the piezoelectric layer. In the specific configuration that is considered herein, the torsional degree of freedom is not influenced by the electric field, and vice-versa. The complete set of aeroelastic equations of the piezoelectric beam reads:

$$\begin{cases} m\ddot{w} + c\dot{w} + kw - \Theta v = L_w \\ I_\vartheta \ddot{\vartheta} + c_\vartheta \dot{\vartheta} + k_\vartheta \vartheta = M_\vartheta \\ C_E v + \Theta w = q \end{cases} \tag{9}$$

Eq. 9 contains the torsional mechanical parameters, namely the torsional inertia I_ϑ, the torsional damping c_ϑ and the torsional stiffness k_ϑ, which have been obtained by introducing a suitable shape function for the torsional rotation:

$$\varphi_1(x_1,t) = \vartheta(t)\psi_\vartheta(x_1) \tag{10}$$

The self-excited aerodynamic lift and moment components are computed on the basis of the Scanlan's expressions[5]:

$$l_w = \frac{1}{2}\rho_f U^2 b\left(KH_1^* \frac{\dot{w}}{U} + KH_2^* \frac{\dot{\vartheta} b}{U} + K^2 H_3^* \vartheta + K^2 H_4^* \frac{w}{b} \right) \tag{11}$$

$$m_\vartheta = \frac{1}{2}\rho_f U^2 b^2\left(KA_1^* \frac{\dot{w}}{U} + KA_2^* \frac{\dot{\vartheta} b}{U} + K^2 A_3^* \vartheta + K^2 A_4^* \frac{w}{b} \right) \tag{12}$$

where $K = b\omega/U$ is the reduced circular frequency, U is the velocity of the fluid flow, ω is the circular frequency of the piezoelectric beam, H_i^* and A_i^* are the flutter derivatives, expressed as dimensionless functions of K.

In order to evaluate the instability condition of the system and the correspondence critical velocity, the following assumption on the governing field is introduced:

$$w = w^* e^{\lambda t}, \quad \vartheta = \vartheta^* e^{\lambda t}, \quad v = v^* e^{\lambda t} \tag{13}$$

so that Eq. 9 is transformed into a quadratic eigenvalue problem (QEP):

$$(\lambda^2 \overline{M} + \lambda \overline{C} + \overline{K}) X^* = 0 \qquad X^* = \begin{pmatrix} w^* & \vartheta^* & v^* \end{pmatrix}^T \tag{14}$$

In Eq. 14, $\overline{M}$, $\overline{C}$ and $\overline{K}$ are the mass, viscous damping and stiffness matrices, respectively. The electro-mechanical coupling is introduced through Eqs. 7 and 8, according to the type of electric external circuit adopted. For RC circuit, by dividing the damping (d) and the stiffness (k) contributions of aeroelastic forces, one finds:

$$\overline{M} = \begin{bmatrix} m & 0 & 0 \\ 0 & I_\vartheta & 0 \\ 0 & 0 & 0 \end{bmatrix} \quad \overline{C} = \begin{bmatrix} c - L_w^d & 0 & 0 \\ 0 & c_\vartheta - M_\vartheta^d & 0 \\ \Theta & 0 & C_E \end{bmatrix} \quad \overline{K} = \begin{bmatrix} k - L_w^k & 0 & -\Theta \\ 0 & k_\vartheta - M_\vartheta^k & 0 \\ 0 & 0 & 1/R \end{bmatrix} \tag{15}$$

Conversely, for RLC circuit:

$$\overline{M} = \begin{bmatrix} m & 0 & 0 \\ 0 & I_\vartheta & 0 \\ \Theta & 0 & C_E \end{bmatrix} \quad \overline{C} = \begin{bmatrix} c - L_w^d & 0 & -\Theta \\ 0 & c_\vartheta - M_\vartheta^d & 0 \\ 0 & 0 & 1/R \end{bmatrix} \quad \overline{K} = \begin{bmatrix} k - L_w^k & 0 & 0 \\ 0 & k_\vartheta - M_\vartheta^k & 0 \\ 0 & 0 & 1/L \end{bmatrix} \tag{16}$$

The problem is solved by transforming (QEP) into an equivalent standard eigenvalue problem (SEP)[11]. The real part of eigenvalues λ stands for the damping component of the system, therefore the flutter instability occurs when this term becomes negative, and the corresponding velocity is the Critical Flutter Velocity.

It is worth noting that, in the case of beams with microscopic size, the Reynolds number attains very low value: Bruno and Fransos[12] have computed, through CFD simulations, the flutter derivatives for a flat plate even for Re = 10. Those functions, reported in Figure 2, are adopted in the present paper.

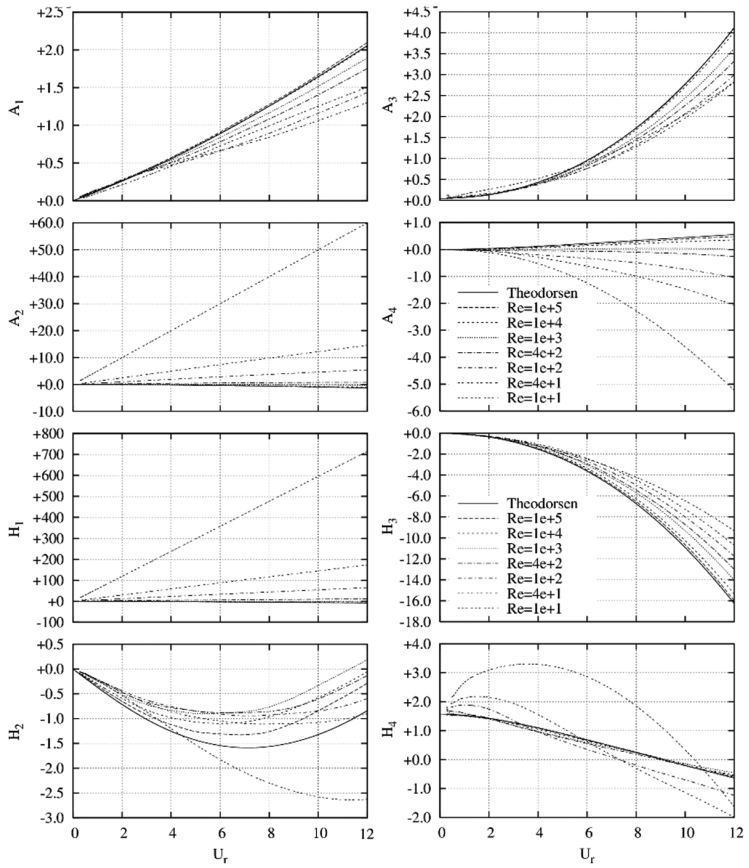

Figure 2: Flutter derivatives computed by Bruno and Fransos for flat plates (adapted from the original paper[12]).

The effects of Reynolds number on aeroelastic behavior of the structure is clear: indeed, when one assumes very small values for *Re*, the difference from the Theodorsen's theory is more marked. According to the trend of the flutter derivatives in Fig. 2, it is possible to make some preliminary considerations on the FI mechanism. For $Re = 10$, the coefficients H_1^* and A_2^* weigh more than the other ones, especially H_1^*; this means that probably the instability occurs according to the transverse degree of freedom. It is important to verify the magnitude of Reynolds number after calculating the critical velocity, as a matter of fact for a variation in the values of *Re* the FI mechanism may change significantly, assuming possibly a coupled translational-torsional behavior.

3. FEATURES OF THE CONSIDERED BEAM

The procedure described in Sec. 2 is applied to a simple cantilever beam, subject to a transverse fluid flow that induces FI. The geometric and constitutive parameters are summarized in Tab. 1. Such a model, which represents a paradigm of realistic devices used as energy harvesters, is used with the purpose of evidence the basic behavior of FI in piezoelectric beams.

The Young's moduli of silicon and PZT are used in order to build the stiffness coefficient of the layered beam; in a similar way, the densities are used for obtaining the mass coefficient; the parameter e_{31} represents the piezoelectric coupling and is adopted in order to obtain Θ; finally, the relative permittivity of PZT, ε_r, is used for computing the capacitance C_E of the piezoelectric layer. The intrinsic bending and torsional damping ratios are assumed, respectively, equal to: $\xi_w = 0.01$ and $\xi_\vartheta = 0.005$. The resistance R and the inductance L of the external circuit are parametrically varied in order to assess their effect on the flutter critical velocity and on the performance of the energy harvester. It is well known from the theory of piezoelectric beams that a non-monotonic effect of the electric parameters is expected[6)10)], with the presence of optimal values which entails the maximum conversion of elastic energy into electric energy.

Table 1: Constitutive and geometric features of the beam studied in this paper.

Parameter	Value	Parameter	Value
ρ_{sil} $[kg/mm^3]$	$2.23 \cdot 10^{-6}$	E_{sil} $[MPa]$	$1.6 \cdot 10^{5}$
ρ_{PZT} $[kg/mm^3]$	$7.83 \cdot 10^{-6}$	E_{PZT} $[MPa]$	$1 \cdot 10^{5}$
$e_{31,PZT}$ $[N/(mmV)]$	$9.33 \cdot 10^{-3}$	$\varepsilon_{r,PZT}$	2400
l $[\mu m]$	200	b $[\mu m]$	25
t $[\mu m]$	8	t_p $[\mu m]$	2

In order to set up the governing system summarized in Eq. 9, the approximating functions for the Rayleigh-Ritz method are defined in this way:

$$\psi_w = \frac{3}{2}\left(\frac{x_1}{L}\right)^2 - \frac{1}{2}\left(\frac{x_1}{L}\right)^3 \qquad \psi_g = \frac{x_1}{L} \tag{17}$$

The cubic approximation, used for the transverse displacement, yields excellent results in terms of the corresponding natural frequency. A very refined, three-dimensional finite element (FE) model has been adopted for establishing a reliable value of the natural frequency for the electro-mechanical system. The one-DOF model adopted herein provide an excellent estimate of the first natural frequency, with a relative error w.r.t the FE solution of less than 0.1%. It is interesting to realize that the 1-DOF model shows a slightly lower frequency than the one for the FE mode, thus suggesting a more compliant behavior. That strange result can be explained by considering that the FE model encompasses three-dimensional effects of piezoelectric behavior, which has the final outcome of increasing the electro-mechanical coupling and, consequently, the natural frequency. For what concerns the torsional vibration frequency, the simple linear model shown in Eq. 17 is not the best option, since it is endowed with a 26.7% relative error w.r.t. the FE model. The situation would be by far better (4% relative error) by considering a cubic function also for the torsional DOF. Nevertheless, in view of the fact that the FI involves the bending DOF only in the present case, the simple approximation of Eq. 17 is retained, because the error on the torsional frequency has no effect on the flutter behavior.

4. CRITICAL FLUTTER VELOCITY

First of all, the case of standard beam, in the absence of piezoelectric coupling, is considered in order to provide the reference value of the critical flutter velocity. in that way, it is possible to give a precise assessment of the effect of piezoelectric coupling for different external circuitry. By considering the first and the second equations in Eq. 9 and by setting to zero the coefficient Θ, one can easily obtain the critical flutter velocity:

$$\bar{U}_{cr} = 3.3 \text{ m/s} \tag{18}$$

The barred symbol stands for the reference value, in the absence of piezoelectric coupling. Account taken of the kinematic viscosity of air ($\nu = 15.35 \cdot 10^{-6}$ m^2/s), one finds that the critical velocity corresponds to the Reynolds number $Re = 1.72$. That number is lower than the minimum value considered in the flutter derivatives, so we have been forced to keep valid the flutter derivatives given for $Re = 10$: this is an important limitation of the present study, even though the final considerations are not largely affected by that fact.

(1) Case of RC circuitry

The electric parameter of the external circuitry has a strong influence on the final damping of the system. Taking into account the damping for the first flexural mode, one finds that the final damping is a non-monotonic function of the parameter $\alpha = \omega_w R C_E$, where $(R C_E)$ is the time constant of charge for the RC circuit. The maximum damping is attained for $\alpha \approx 1$, with a 60% increase w.r.t. the initial value of purely mechanical damping. This means that the condition $R \approx 1/(\omega_w C_E) \approx 30\ \Omega$ should hold in order to obtain, for

the considered beam, the optimal external circuit. In Fig. 3 the real and imaginary part of the eigenvalues for the cantilever are plotted. The analyses are performed considering three different values of load resistance. In all the cases the instability occurs for the transverse degree of freedom. The trend of damping ratio follows that obtained in the purely mechanical case, related to the H_1^* coefficient. The load resistance does not affect the natural frequency of the structure, which remains almost constant (as it happens in the absence of electro-mechanical coupling). Tab. 2 shows the electro-mechanical damping ratio and the critical fluid velocity. It can be seen a substantial increase in both quantities w.r.t. the absence of electro-mechanical coupling. That behavior is expected, since the piezoelectric effect entails an increase of damping, due to the conversion of mechanical energy into electrical one, so that the fluid velocity to reach FI is increased. When $R = 30\ \Omega$ the damping and the flutter speed achieve their maximum.

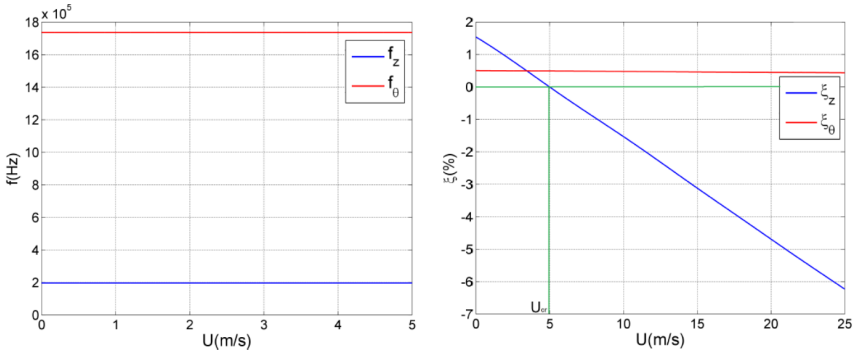

(a) *Frequency trend.* (b) *Damping trend for R=20 Ω.*

(c) *Damping trend for R=30 Ω.* (d) *Damping trend for R=100 Ω.*

Figure 3: Results of FI analyses for the considered cantilever, RC circuitry with various load resistances.

Table 2: Synopsis of the results and comparison with no electro-mechanical coupling (RC circuitry).

R [Ω]	ξ_w [-]	$\Delta\xi_w$	U_{cr} [m/s]	ΔU_{cr}	Re_{cr}
20	0.0154	54%	5.0	52%	2.61
30	0.0160	60%	5.1	54%	2.66
100	0.0131	31%	4.3	30%	2.24

(2) Case of RLC circuitry

In this case, there is also the complex eigenvalue associated to the voltage field, in agreement with the non-singularity of the matrix of the masses. Like for the RC circuit the influence of electric parameters on the transverse damping ratio is evaluated. The results show a maximum at the condition $\eta = 1$, where $\eta = \omega^2_w L C_E$; this means that the damping is amplified when the mechanical part of the system is synchronized with electric one. On the other hand, the effect of resistance shows a different peak in function of the value of

inductance and of the electro-mechanical coupling coefficient. In general, one can notice that the increase of damping for RLC circuitry is by far larger than in the previous case: the final damping is up to 8 times larger than the initial mechanical damping.

Fig. 4 shows the evolution of frequency and damping for each field, by introducing the aeroelastic component. The value of inductance is taken in order to match the circular natural frequency of the mechanical part to the frequency of the electrical circuitry (L = 0.024 mH), so that the mechanical damping is maximized. The analysis is performed for three different load resistances, see Tab. 3. As expected, the magnitude of equivalent damping for $U = 0$ is much larger compared to the RC circuit and this aspect is reflected in the magnitude of flutter velocity, which considerably increases. In the considered cantilever ξ_w assumes its maximum for R = 100 Ω, but U_{cr} is higher for R = 150 Ω, achieving values much larger than the purely mechanical case. It is interesting to notice that in this case the damping ratio shows a different decay w.r.t. to what happens for the RC circuit and the simple mechanical problem. This behavior is more accentuated for R = 100÷150 Ω. The plot in Fig. 4 presents an initial velocity range in which the electrical and mechanical damping follow the same trend, then, by increasing the fluid speed, the slope of electrical response changes sign in contrast to the mechanical response. The order of magnitude of Reynolds number, in agreement with the increase of critical flutter velocity, is higher, reaching for R = 100÷150 Ω, suitable values in order to consider appropriate the set of flutter derivatives assumed in this analysis.

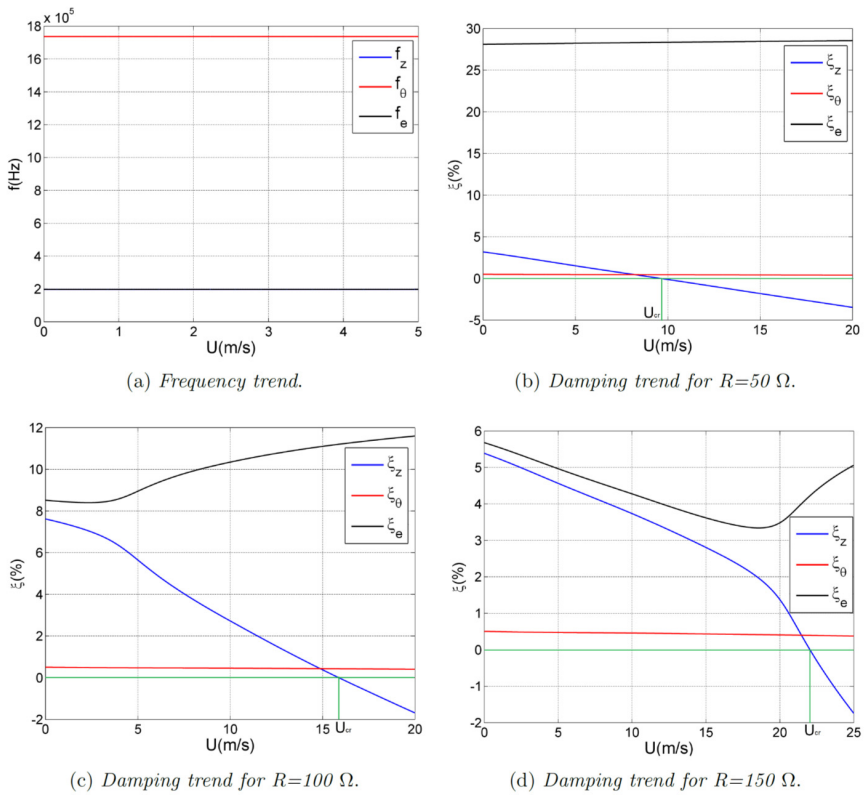

(a) *Frequency trend.* (b) *Damping trend for R=50 Ω.*

(c) *Damping trend for R=100 Ω.* (d) *Damping trend for R=150 Ω.*

Figure 4: Results of FI analyses for the considered cantilever, RLC circuitry with various load resistances.

Table 3: Synopsis of the results and comparison with no electro-mechanical coupling (RLC circuitry).

R [Ω]	ξ_w [-]	$\Delta\xi_w$	U_{cr} [m/s]	ΔU_{cr}	Re_{cr}
50	0.0320	220%	9.6	190%	5.00
100	0.0762	662%	15.9	381%	8.28
150	0.0540	440%	22.0	567%	11.47

5. APPLICATION TO ENERGY HARVESTING

In this chapter, the possibility to exploit aeroelastic effects for energy harvesting purposes is evaluated. However, being flutter essentially an unstable phenomenon, it is necessary to integrate another exciting component that ensures a continuous supply of energy, e.g. an inertial system. In order to understand how FI affects the behavior of the energy harvesting system, the time-variant evolution is computed for the cantilever subject to the fluid flow and to an initial tip displacement equal to the thickness of the beam. In this way, we consider the dynamic response to an impulsive excitation of the beam. Such a situation is quite common if the energy harvester is used in conjunction with a frequency-up conversion device[13]. The structure is studied considering the two different electric circuit, with resistance and inductance that maximize the mechanical damping. This means, for RC circuitry, that $R = 30\ \Omega$ and for RLC circuit that $L = 0.024$ mH and $R = 100\ \Omega$. The aeroelastic effect is included by considering a fluid speed slightly smaller than the critical value computed in Sec. 4: RC circuit $U = 5$ m/s; RLC circuit $U = 15$ m/s.

(1) Case of RC circuitry

The aeroelastic mechanism affects significantly the response of the system. According to the magnitude of coefficient A_2^*, the torsional rotation is not affected by the aeroelastic behavior. On the other hand the tip displacement presents a much less damped response considering the fluid effect. This aspect is reflected on the voltage due to the electro-mechanical coupling and consequently on the harvested power trend (see Fig. 5). The reduction of damping, however, does not affect the peak amplitude of the harvested power, that remains practically the same, contrary to what happens for RLC circuit as discussed in the following section. It is important to mention that the overall harvested energy is largely increased, because of the slow oscillation decay.

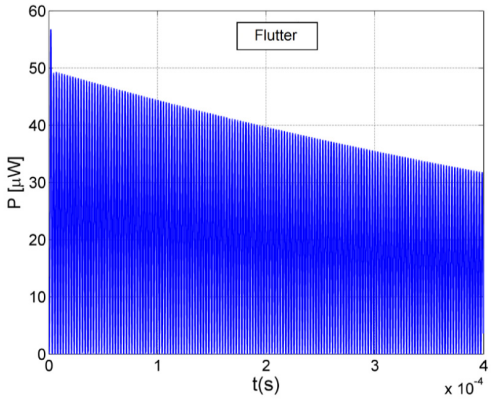

Figure 5: Dynamic response of the cantilever, RC circuit, $R = 30\ \Omega$, $U = 5$ m/s.

(2) Case of RLC circuitry

Also in this case, the dynamic response is largely affected by the aeroelastic effect, showing larger oscillation amplitude. Compared to the purely resistive solution, in this case the harvested power achieves an amount much larger: the peak power is on orders of magnitude higher than in the RC circuit (see Fig. 6). We can conclude that, for RLC circuitry, the reduction of the mechanical damping affects not only the decay of the response (i.e. the overall harvested energy), but also the maximum amplitude (i.e. the peak power).

5. CONCLUSIONS

In the present paper, we show the application of flutter analysis to piezoelectric beams in MEMS, with the main purpose of exploring the possible application of energy harvesting in the presence of aeroelastic effects. The results, computed on the basis of the dynamic solution of the fully coupled problem, demonstrate the possibility to exploit the flutter mechanism to improve an energy harvesting device. The advantages are linked to the considerable reduction of the mechanical damping. The relatively small critical velocities make it possible to adopt these devices anywhere in the surrounding environment. As previously mentioned, it is

necessary to point out that the device must still integrate another exciting source, as the flutter is just an instability mechanism.

One important aspect for MEMS is the low Reynolds number. Despite the increase of the flutter critical speed for piezoelectric coupling, the magnitude of the Reynolds number still fails to achieve the value $Re = 10$, which is the minimum value for the flutter derivatives in literature. For this reason, the results could be slightly altered. To comply with this problem it would be better to evaluate, through CFD analyses[14], a more accurate set of aerodynamic coefficient, applicable to this particular structure.

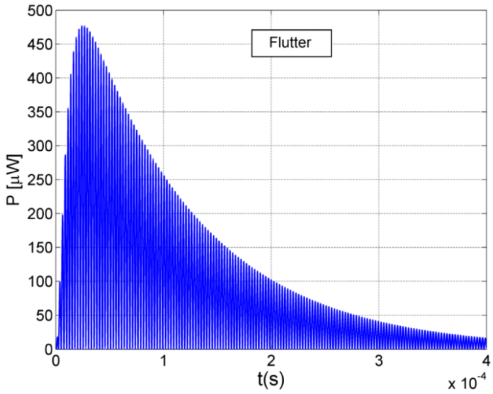

Figure 6: Dynamic response of the cantilever, RLC circuit, $L = 0.024$ mH, $R = 100\ \Omega$, $U = 15$ m/s.

REFERENCES

1) Jacobsen, H., Prume, K., Wagner, B., Ortner, K., and Jung, T. : High-rate sputtering of thick PZT thin films for MEMS. *J. of Electroceramics*, Vol. 25, pp. 198-202, 2010.
2) Kim, S.-G., Priya, S., and Kanno, I. : Piezoelectric MEMS for energy harvesting. *MRS Bulletin*, Vol. 37, pp. 1039-1050, 2012.
3) Jeon, Y., Sood, R., Jeong, J.-H., and Kim, S.-G. : MEMS power generator with transverse mode thin film PZT. *Sens. Act., A: Phys.*, Vol. 122, pp. 16-22, 2005.
4) Ardito R., and Musci R.: MEMS energy harvesters based on aeroelastic phenomena, *Proc. of the 11th World Congress on Computational Mechanics (WCCM)*, Barcelona, Spain, 2014
5) Scanlan, R.H., and Simiu, E. : *Wind effects on Structures*, John Wiley and Sons Inc., 3rd edition, 1996.
6) Gafforelli, G., Corigliano, A., and Ardito, R.: Improved one-dimensional model of piezoelectric laminates for energy harvesters including three dimensional effects. *Compos. Struct.*, Vol. 127, pp. 369-381, 2015.
7) Ballhause, D., D'Ottavio, M., Kröplin, B., and Carrera, E.: A unified formulation to assess multilayered theories for piezoelectric plates. *Computers & Struct.*, Vol. 83, pp. 1217-1235, 2005.
8) IEEE Standard on Piezoelectricity. *The institute of Electrical and Electronics Engineers*, 1987.
9) Ardito, R., Bertarelli, E., Corigliano, A., and Gafforelli, G. On the application of piezolaminated composites to diaphragm micropumps. *Compos. Struct.*, Vol. 99, pp. 231-240, 2013.
10) Renno, J.M., Daqaq, M.F., and Inman, D.J.: On the optimal energy harvesting from a vibration source. *J. Sound Vibr.*, Vol. 320, pp. 386-405, 2009.
11) Ardito, R., Comi, C., Corigliano, A., and Frangi, A.: Solid damping in micro electro mechanical systems. *Meccanica*, Vol. 43, pp. 419-428, 2008.
12) Bruno, L., and Fransos, D.: Evaluation of the Reynolds number effects on the flutter derivatives of a flat plate by means of a new computational approach, *J. Fluid Struct.*, Vol. 24, pp. 1058-1076, 2008.
13) Ardito, R., Corigliano, A., Gafforelli, G, Valzasina, C., Procopio, F., and Zafalon, R.: Advanced model for fast assessment of piezoelectric micro energy harvesters. *Frontiers in Materials*, in press, 2016.
14) Le Maître, O.P., Scanlan, R.H., and Knio, O.M.: Estimation of the flutter derivatives of an NACA airfoil by means of Navier-Stokes simulations, *J. Fluid Struct.*, Vol. 17, pp. 1-28, 2003.